# Functional and Morphologic Analysis of the Fluid-Conducting Meshwork in Xenografted Cutaneous and Primary Uveal Melanoma

*Ruud Clarijs, Marcory van Dijk, Dirk J. Ruiter, and Robert M. W. de Waal*

**Purpose.** In primary uveal and cutaneous melanoma lesions, extracellular matrix (ECM) is often deposited in arcs, loops, and network patterns. Based on prognostic relevance, these patterns appear to play a significant role in facilitating metastasis. It has been demonstrated that these patterns were capable of transmitting fluid. The current study was undertaken to elucidate further the functional role of these patterns in tumor perfusion and to examine the composition of the patterns by immunohistochemistry.

**Methods.** To study the role of these patterns in perfusion, fluorochrome-labeled bovine serum albumin, bovine insulin, and dextrans of different molecular sizes were injected intravenously into nude mice bearing subcutaneous human cutaneous melanoma xenografts. Distribution of the human melanoma cells and murine host cells was analyzed by DNA in situ hybridization. To elucidate the composition of these patterns, human uveal melanoma tissues were analyzed for expression of ECM components by immunohistochemistry.

**Results.** Small molecules (Stokes' radius $<4.4$ nm) crossed the vessel wall and spread along the ECM patterns within 2 to 10 minutes, whereas larger molecules (Stokes' radius $\sim 5.8$ nm) required 30 to 45 minutes to enter. Murine host cells were found exclusively in the ECM pattern compartment. In primary uveal melanoma, different types of collagen, ECM-associated heparan sulfate proteoglycans, and different types of cells were present in the patterns.

**Conclusions.** The data suggest that the ECM deposited as arcs, loops, and network patterns, accommodate the transport of plasma-derived molecules, (e.g., nutrients), to the tumor lesion, thus enhancing tumor growth and progression, and facilitating infiltration of tumor tissue by host-derived cells. (*Invest Ophthalmol Vis Sci.* 2005;46:3013–3020) DOI:10.1167/iovs.04-0876

In both primary uveal and cutaneous melanoma, nine different patterns of extracellular matrix (ECM) deposition have been identified by conventional periodic acid-Schiff (PAS) staining.[1–4] Analysis of prognostic relevance indicated that the PAS-positive arcs, loops, and network patterns are associated with tumor progression and subsequent poor survival.[1–5] A few years ago, it was suggested that these patterns contained or represented blood-conducting channels lined by tumor cells instead of endothelial cells (vasculogenic mimicry).[6] Since then, findings in several studies have suggested that vasculogenic mimicry occurs in different tumor types and have identified the factors causing this phenomenon (for review, see Ref. 7).

Recent studies have reported the presence of laminin and collagen I and VI in,[8,9] and different types of cells (including endothelial cells and macrophages) along the PAS-positive arcs, loops, and network patterns.[8,10,11] Macrophages in malignant tumors, including uveal melanoma, have been associated with adverse prognosis,[10–14] although their mechanism of action is unknown. Heparan sulfate proteoglycans (HSPGs) and other structural proteins, which are key components of the ECM (such as collagen III and V), may also be of significance in tumor growth and metastasis.

In a recent study,[8] we reassessed the nature of the PAS-positive patterns in primary uveal and xenografted melanoma. We and others[15] have suggested that a fluid stream may be present in these ECM depositions, apart from the blood circulation. This fluid-conducting meshwork was found in areas with a relatively low vascular density but without evident necrosis,[16] indicating that it may play a role in tumor cell nutrition. Indeed, the importance of this meshwork was recently emphasized by Hendrix et al.[7] If this meshwork is involved in tumor cell nutrition, the questions arises of which nutrients are delivered to the tumor cells. In our previous study,[8] we showed that bovine serum albumin is capable of entering the patterns in less than 1 hour. Indeed, these data may indicate that small-sized molecules (such as glucose and oxygen) are capable of leaving the blood vessels and being transported through the patterns within a few minutes, thereby contributing to tumor growth and metastasis.

To elucidate the properties of the ECM arcs, loops, and network patterns, we have now analyzed their ability to transport tracer molecules, studied details of their composition, and determined the presence of associated cell types in xenografted cutaneous melanoma and in primary uveal melanoma. For this purpose, we selected several tracers with a range of molecular sizes—the smallest being representative of small nutrient molecules (expected to distribute widely along the patterns after a short time interval), the middle sizes being indicative of endothelial permeability changes (expected to distribute along the patterns after a larger time interval), and the largest assumed to be purely intravascular (i.e., not entering the patterns outside the vasculature and the vascular channels, if present).

From the Department of Pathology, Radboud University Nijmegen Medical Centre, Nijmegen, The Netherlands.

Supported by Grant 98-1816 from the Dutch Cancer Society.

Submitted for publication July 26, 2004; revised February 9 and April 26, 2005; accepted May 3, 2005.

Disclosure: **R. Clarijs**, None; **M. van Dijk**, None; **D.J. Ruiter**, None; **R.M.W. de Waal**, None

The publication costs of this article were defrayed in part by page charge payment. This article must therefore be marked "*advertisement*" in accordance with 18 U.S.C.§1734 solely to indicate this fact.

Corresponding author: Ruud Clarijs, Department of Pathology, Radboud University Nijmegen Medical Centre, PO Box 9101, 6500 HB Nijmegen, The Netherlands; r.clarijs@pathol.umcn.nl.

**TABLE 1.** Primary Antibodies Used for Immunohistochemistry

| Primary Antibody | Marker Specificity | Source of Antibody/Reference |
|---|---|---|
| Mec 7.46 | CD31 (endothelial cells) | Hycult Biotechnology, Uden, The Netherlands |
| Anti-laminin* | Laminin | Dr. J. van den Born, Department of Nephrology, UMC Nijmegen, The Netherlands |
| 3G10 | Pan-HSPG | 21 |
| JM403 | Heparan sulfate side chains | 22 |
| 10H4 | Syndecan-2 | 23, 24 |
| 2E9 | Syndecan-1 and -3 | 24, 25 |
| 1C7 | Syndecan-3 | 24, 25 |
| S1 | Glypican-1 | 26, 27 |
| JM72 | Agrin | 28 |
| 1948 | Perlecan | Chemicon International Inc, Temecula, CA |
| Anti-all hu XVIII | Both collagen XVIII | 29 |
| (QH48.18) | Variants | 30 |
| L26 | CD20 (B-lymphocytes) | DAKO, Glostrup, Denmark |
| Anti-leu-4 | CD3 (T-lymphocytes) | BD Biosciences, San Jose, CA |
| Anti-collagen I* | Collagen I | Monosan, Uden, The Netherlands |
| Anti-collagen III* | Collagen III | Monosan |
| Anti-collagen IV | Collagen IV | Sigma-Aldrich, Brunschwig, Amsterdam, The Netherlands |
| Anti-collagen V | Collagen V | Monosan |
| HHF35 | Isotypes of actin ($\alpha$, $\gamma$) (smooth muscle cells, pericytes) | Dako, 31, 32 |

All antibodies were applied in uveal melanoma except for Mec 7.46, which was applied in xenografted melanoma.
* polyclonal antibodies

## MATERIALS AND METHODS

### Uveal Melanoma

Frozen specimens of six uveal melanoma lesions were obtained from the pathology archives of the University Medical Center Nijmegen where they had been stored at −130°C. Tissues were used according to the guidelines of Dutch legislation, and our work adhered the tenets of the Declaration of Helsinki. All specimens were stained by Azan histochemistry for visualization of the ECM patterns.[8,17] Three melanomas contained arcs, loops, and network patterns and were selected for further analysis.

### Xenografts in Nude Mice

Because there are close parallels in PAS and Azan histochemistry of the arcs, loops, and network patterns in cutaneous Mel57-xenografts and primary uveal melanoma,[8] the human cutaneous melanoma cell line Mel57[18] was cultured as previously described.[19] For the induction of tumor growth, $2.5 \times 10^6$ cells were injected subcutaneously into the flanks of BALB/c *nu/nu* mice ($n = 76$). Subcutaneous xenografts developed in all mice. Tumor volumes were estimated by multiplying length, width, and height. When the tumors reached sizes between 100 and 700 $mm^3$, all mice were injected intravenously with 100 $\mu$L of tracer solution (described in the next section). Tumors were excised at 2, 10, 15, 30, and 45 minutes or at 1, 3, or 24 hours after injection. Subsequently, tumors were divided into two parts. One part was snap frozen in liquid nitrogen, and the other part was formalin fixed. Two animals were included per tracer type and time point. Our work adhered to the ARVO Statement for the Use of Animals in Ophthalmic and Vision Research and was approved by an institutional review board (Dier Experimenten Commissie).

### Tracers

Tracers with a broad range of molecular size were selected. A 3% (wt/vol) solution of bovine serum albumin (BSA) labeled with fluorescein isothiocyanate (FITC-BSA, molecular mass approximately 68 kDa; 12 moles FITC/mole BSA), with sulforhodamine 101 acid chloride (Texas red-BSA; 3 moles Texas Red/mole BSA), or with biotin (8–16 moles biotin/mole BSA) was injected intravenously. In addition, 6% (wt/vol) of FITC-labeled bovine insulin (FITC-I; 1 mole FITC/mole insulin, molecular mass approximately 5.8 kDa) and 1%, 2%, 3%, and 6% (wt/vol) solutions of FITC-labeled dextrans (FITC-D; 0.003–0.02 mole FITC/mole glucose) with average molecular weights of 20,000 (FITC-D20), 40,000 (FITC-D40), 70,000 (FITC-D70), and 2,000,000 (FITC-D2000) were also tested. We selected these tracers because they were representative of small nutrient molecules (i.e., FITC-I, FITC-D20, and FITC-D40) or were indicative of endothelial permeability changes (i.e., FITC-D70, FITC-BSA), or assumed to be purely intravascular (i.e., FITC-D2000). All tracers were obtained from Sigma-Aldrich Brunschwig (Amsterdam, The Netherlands).

To determine the optimal conditions for studying tumor perfusion, we first injected nude mice carrying melanoma xenografts intravenously with 3% labeled BSA; 6% FITC-I; or 1%, 2%, 3%, or 6% FITC-D70 and evaluated tracer distribution in the tumor tissue after 2 minutes (in the case of FITC-I) or 30 and 60 minutes (in the cases of labeled BSA and FITC-D70, respectively). The distribution of FITC-BSA and FITC-I was readily detectable in all xenografts (Fig. 1B), as shown previously for FITC-BSA.[8,20] After perfusion with Texas red-BSA, fluorescence was hardly detectable (not shown). Histochemical visualization of biotin-BSA was unsuccessful as well, because of a high background (not shown). With 6% FITC-D70, there was reproducible visualization of tracer distribution on fresh cryosections (not shown). Therefore, 3% FITC-BSA, 6% FITC-I, and 6% FITC-D solutions were used for further study.

### Immunofluorescence

Cryosections (4 $\mu$m) of xenografts containing FITC-BSA were fixed in acetone for 10 minutes. Binding of anti-CD31 monoclonal antibody (mAb) Mec 7.46 (Table 1) was detected by secondary tetramethylrhodamine isothiocyanate (TRITC)–labeled antibodies (Alexa Fluor 568; Molecular Probes, Leiden, The Netherlands). In the same section, binding of anti-laminin polyclonal antibodies (Table 1) was detected by a secondary Cy 5-labeled anti-rabbit antibody (GE Healthcare Ltd., Buckinghamshire, UK). Nuclear counterstaining was performed by incubating the sections for 1 minute in 4′,6-diamidino-2-phenylindole solution (DAPI, 0.2 mg/mL; Sigma-Aldrich) and mounted in antifade medium (VectaShield; Vector Laboratories Inc., Burlingame, CA). In the case of xenograft perfusion with FITC-I or -D, tracer distribution was directly visualized in an unfixed 4-$\mu$m cryosection. Images were

collected and digitally stored. Subsequently, sections were fixed and double stained.

Distributions of CD31 and laminin were visualized and digitally stored as well. To evaluate tracer distribution, digital images before and after double staining were exactly matched to be able to evaluate tracer in the entire tissue section. For all tracers studied, their presence in (CD31-positive) blood vessels and (laminin-positive) ECM patterns was evaluated. The amount of tracer present was compared in a semiquantitative way by comparing the amount of tracer between the different time points per tracer type. The amount of tracer at a certain time point in the two corresponding xenografted lesions was averaged and related to the highest amount of tracer per tracer type.

### In Situ Hybridization

Three xenografted tumors were used for DNA in situ hybridization analysis. The 4-$\mu$m paraffin-embedded sections were deparaffinized, rehydrated, and immersed in 3% $H_2O_2$ in phosphate-buffered saline for 30 minutes. Subsequently, sections were incubated for 10 minutes in 1 M sodium thiocyanate at 80°C, and protein digestion was performed for 15 minutes in pepsin dissolved in distilled water (400 U/mL, pH 2.0). Sections were dehydrated and air dried before hybridization. Total DNA was isolated from human whole blood and murine kidney and liver tissue (Puregene DNA isolation kit; Gentra, Minneapolis, MN). Human DNA was labeled with biotine-16-dUTP with a nick translation mix (Roche Diagnostics GmbH, Mannheim, Germany) and murine DNA with digoxigenin-11-dUTP (Roche Diagnostics GmbH). Both probes (each probe: 3.3 ng/$\mu$L) were mixed in hybridization buffer (62.5% formamide, 10% dextran sulfate, 2× sodium citrate-Tween [pH 7.0]) and denatured at 72.5°C for 5 minutes. Sections were hybridized overnight at 42°C. Subsequently, sections were washed at 45°C for 15 minutes with a solution of 50% formamide and 2× saline sodium citrate (pH 7.0) and in phosphate-Nonidet buffer (10 mM/L $Na_2HPO_4$, 10 mM $Na_2H_2PO_4$, and 0.5% Nonidet P-40 detergent) for 10 minutes at room temperature. Biotin-labeled human DNA was detected with mouse anti-biotin polyclonal antibodies (pAbs; diluted 1:100; Dako, Glostrup, Denmark), alkaline phosphatase-conjugated avidin-biotin complex (ABC; Vectastain; Vector Laboratories), and visualized by incubation with a mixture of 1 mg/mL fast blue, 0.2 mg/mL naphthol phosphate, and 0.24 mg/mL levamisole (Sigma-Aldrich) for 10 minutes. Digoxigenin-labeled mouse DNA was detected with mouse anti-digoxigenin pAbs (dilution 1:50; Roche Diagnostics GmbH) and horseradish peroxidase (HRP; EnVision system; Dako), and developed by a 10-minute incubation with a 0.4 mg/mL amino-9-ethyl-carbazole solution (Aldrich, Steinheim, Germany). Sections were then mounted (Imsol; Klinipath B.V., Duiven, The Netherlands).

### Immunohistochemistry

Antibodies used for immunohistochemistry are listed in Table 1. The distribution of all included markers and biotin-BSA was evaluated in a standard three-step ABC method (Vectastain; Vector Laboratories) and developed in 3-amino-9-ethyl-carbazole. Before they were immunostained, strongly pigmented sections were selected and bleached by incubation with 3% (vol/vol) hydrogen peroxide and 1.0% (wt/vol) disodium hydrogen phosphate for 18 hours at room temperature. For staining with the 3G10 mAb, directed against heparitinase-digested HSPGs, sections were pretreated with 50 mU heparitinase (heparinase III, EC 4.2.2.8; Sigma-Aldrich). All sections were counterstained for 45 seconds with Harris' hematoxylin (Merck, Darmstadt, Germany) at room temperature. Finally, reticulin was detected by Laguesse histochemistry, and the sections mounted (Imsol mounting medium; Klinipath B.V.).

## Results

### Tracer Studies

Tracer localization was determined by comparing its distribution with laminin (ECM patterns) and CD31 (microvasculature) immunofluorescence, as described previously.[8] In all cases, mice used per tracer type and per time point showed similar distributions of tracer, allowing reliable comparison. Tracer ability to enter the ECM was dependent on molecular size: FITC-BSA spread in approximately 45 minutes (not shown). FITC-I entered the patterns within 2 minutes (Figs. 1A–C). FITC-D70 infiltrated in the same time as FITC-BSA (Fig. 1J), whereas FITC-D20 and FITC-D40 appeared after 10 minutes (Figs. 1D–F, 1J). In particular with FITC-I and FITC-D20, a diffuse staining pattern was seen, indicating that these tracers had penetrated the tumor nests as well. The large molecular size marker FITC-D2000 extravasated perivascularly and was observed occasionally close to large vessels (Figs. 1G–I). Remarkably, at 24 hours after injection FITC-BSA was still present in the patterns, whereas FITC-D of any size had completely disappeared. When we incubated a 3% FITC-BSA solution for 1 hour on 4-$\mu$m unfixed cryosections of three xenografts, it appeared that FITC-BSA had bound to the ECM patterns directly and, to a lesser extent, to the tumor cells as well (not shown).

### In Situ Hybridization of Xenografted Tumors

In situ hybridization analysis of both human and mouse total DNAs showed the localization of human tumor cells and associated murine stromal cells in melanoma xenografts. Apart from intravascular white blood cells and endothelial cells, host cells were present predominantly along the ECM patterns, whereas infiltration between tumor cells was rare (Fig. 2).

### Morphologic Analysis of the ECM Patterns in Uveal Melanoma

To investigate the composition of the ECM patterns and to study effects of the presence of such patterns on the localization of infiltrating immune cells in uveal melanoma, immunohistochemical analysis was performed with a panel of antibodies that have well-documented specificity (Table 1). Results are listed in Table 2. Except for weak staining of collagen III in the microvasculature, all tested subtypes of collagen showed evident staining (Figs. 3A–D). The basement membrane-associated HSPGs agrin (Fig. 3E) and perlecan (Fig. 3F) were found in the ECM patterns and surrounding the vasculature, whereas expression of the cell membrane-associated HSPGs syndecan-1 and -3 (Fig. 3G), syndecan-2 (Fig. 3H), and glypican-1 (Fig. 3I) was weak and mainly restricted to tumor cells. Occasionally, syndecan-1,-3 and syndecan-2 (Figs. 3G, 3H) were expressed by pattern-associated cells, probably macrophages, as shown previously.[33] Reticulin was also present in the ECM patterns (Fig. 3J). Actin-positive pericytes were mostly confined to larger vessels (Fig. 3K).

Infiltrate analysis showed that a few B-lymphocytes were present around major vessels at sites of dense infiltration (Fig. 3L). T-lymphocytes were also present in the perivascular infiltrates but were occasionally found along the patterns in uveal melanoma (Fig. 3M).

## Discussion

Several studies[6,7,15,34,35] have shown that only highly aggressive melanoma cells generate ECM patterns in vitro, indicating an essential role of these patterns in tumor progression. In-

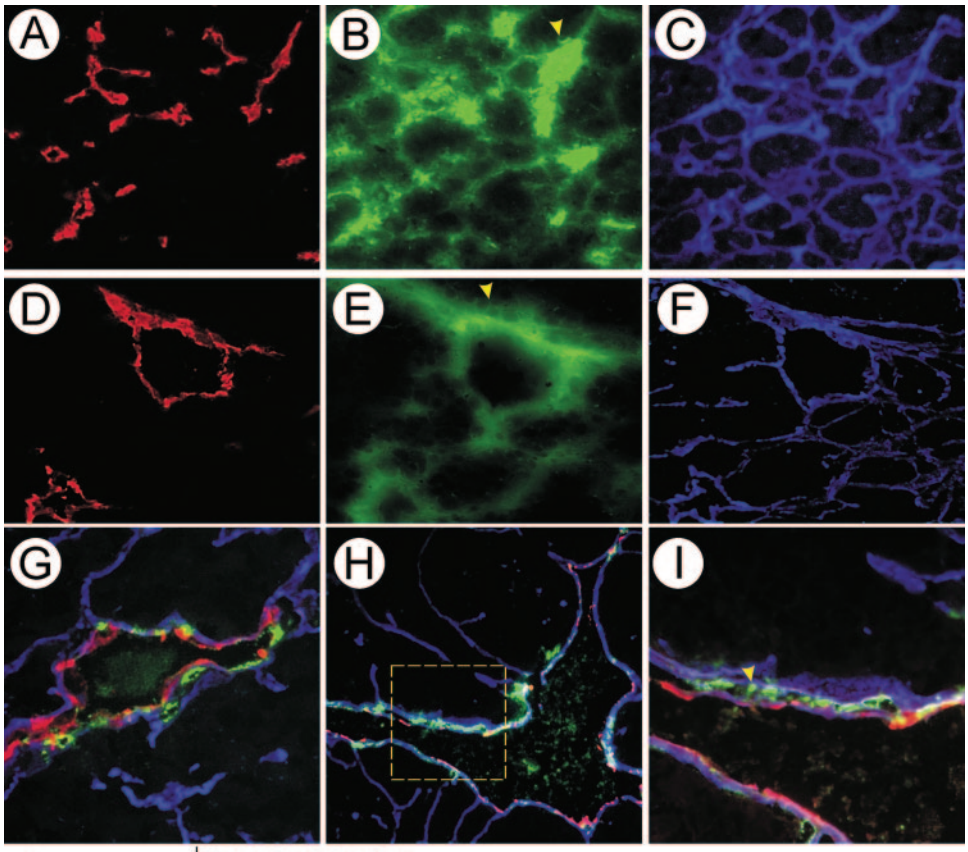


J

| Tracer | Time after injection | | | | | | | |
|---|---|---|---|---|---|---|---|---|
| | 2 min | 10 min | 15 min | 30 min | 45 min | 1 h | 3 h | 24 h |
| FITC-BSA | NT | | | | | | NT | |
| FITC-I | | NT | NT | NT | NT | NT | NT | NT |
| FITC-D20 | | | | | NT | NT | NT | NT |
| FITC-D40 | | | | | | | NT | NT |
| FITC-D70 | NT | | | | | | | |
| FITC-D2,000 | NT | | NT | | NT | | NT | |

**FIGURE 1.** Distribution of FITC-I (**B**) and FITC-D20 at 2 minutes (**E**) and FITC-D2000 at 10 (**G**) and 60 (**H**, **I**) minutes after intravenous injection. Endothelial cells were detected by CD31 (*red*; **A**, **D**, **G–I**) and the ECM patterns by laminin (*blue*; **C**, **F**, **G–I**) immunofluorescence. Distribution of FITC-D2000, CD31, and laminin have been digitally superimposed. FITC-I and FITC-D20 rapidly distributed in- and outside the vasculature along the ECM patterns. The fuzzy fluorescence pattern seen with FITC-I or FITC-D20 may indicate leakage between tumor cells outside the ECM patterns (**B**, **E**; *arrowheads*). (**E**) Tumor cell nuclei are visible (*arrowhead*). To show FITC-D2000 in more detail, tracer distribution in the *boxed area* (**H**) containing a large vessel is depicted in the *boxed area* in (**I**). FITC-D2000 leaked into the perivascular space, probably to the level of the pericytes (**I**, *arrowhead*). (**J**) Tracer distribution data in the time course after intravenous injection are summarized. *Dashed cells*: intra- or directly perivascular presence of tracer (as shown in **E**); *gray-to-black–filled cells*: amounts of tracer present in the ECM patterns (as shown in **D**, **E**, **G–I**). *Unfilled cells*: absence of tracer. NT, not tested. Magnification: (**A–H**) ×400; (**I**) ×200.

deed, as shown by these studies, the presence of blood-conducting channels in these patterns may be essential for development of this phenomenon. However, we did not observe these nonendothelial cell–lined tubes conducting blood in our xenograft model.[8] Theoretically, there are additional possible explanations for the effects of the ECM arcs, loops, and network patterns on tumor progression in uveal melanoma: (1) The matrix deposits facilitate angiogenesis by guiding endothelial cell migration; (2) they facilitate access of plasma-derived molecules to the tumor cells; (3) they facilitate infiltration of tumor tissue by macrophages, which, in turn, enhance angiogenesis[36]; (4) they facilitate escape of tumor cells from the primary tumor lesion; and (5) matrix deposition is merely a side-effect of tumor progression. In line with the second explanation, we recently reported that the ECM patterns may represent a fluid-conducting meshwork (Fig. 4A). Functional evaluation of this meshwork by fluorochrome-labeled insulin, BSA, and dextrans of different sizes indicated that there is a rapid entrance into the patterns of particles with a Stokes' radius of 4.4 nm or less (based on the molecular weight of FITC-D40, using the method of Granath and Kvist[39]) within 2 to 10 minutes, whereas penetration of larger particles (Stokes' radius >5.8 nm [FITCD-70]) took approximately 30 to 45 minutes. In addition, some leakage of FITC-I and FITC-D20 of small molecular size from the ECM patterns between the tumor cells lining these patterns occurred (Fig. 4B). The exact nature of this transport is unclear: Fluid may be transported by an actual current or by diffusion and convection.[40] Our data are in line with either a process of diffusion and convection,[40] or with a stream of molecules of limited size, comparable to pressure-driven filtration (Fig. 4). Entrance of fluid derived from the blood into the patterns is determined by the permeability of the endothelium and the compactness of the ECM. Leakage of FITC-D2000 was mainly restricted to the perivascular space, indicating that entrance of particles with a Stokes' radius of at least 27.9 nm, is mainly determined by ECM composition.

Our tracer data imply that nutrients can be transported relatively rapidly via the ECM patterns toward tumor cells located at some distance from blood vessels. Hence, in primary uveal melanoma, the role of the fluid-conducting meshwork may be essential for survival of tumor cells and may explain why necrosis is absent in areas that contain ECM patterns but have low vessel density.[16] Although tumor vessels leak macromolecules in many experimental and human solid tumors, extravasation of these molecules is often poor. This may be

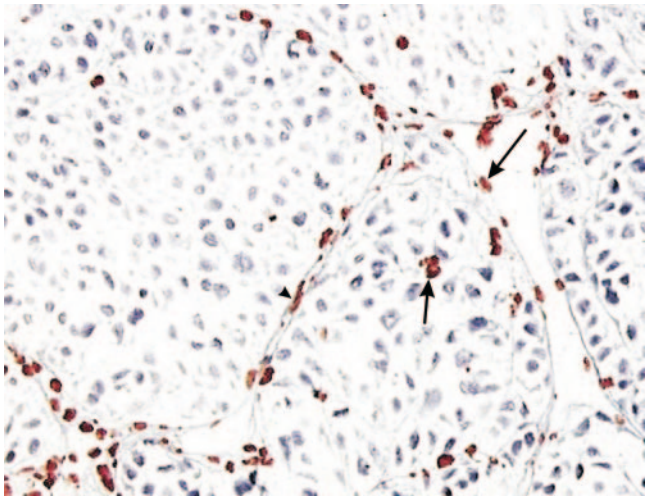

**FIGURE 2.** DNA in situ hybridization analysis of a melanoma xenograft lesion using total human DNA (*blue*) and total murine DNA (*red*) for simultaneous differential detection of human and murine cells. Murine cells were associated with the ECM patterns (*arrowhead*) and formed the endothelial lining of the microvasculature (*arrow* in vessel lumen). Sporadically, murine cells seemed to infiltrate tumor cells nests (*short arrow*). Magnification, ×400.

explained by the high interstitial fluid pressure in the center of a tumor.[37] This phenomenon is of significance in the design and application of therapeutic agents. However, in the case of tumors containing ECM patterns, these structures may provide a gateway for the delivery of therapeutic agents into the tumor lesion. Thus, although the patterns may be involved in tumor cell nutrition and progression on the one hand, their presence may contribute to efficient therapy on the other. In this respect, a possible effect on immunotherapy is supported by a previous study showing that intravenous injection of specific monoclonal antibodies and FITC-D in melanoma-bearing mice resulted in similar distribution patterns.[41]

In this and a previous study,[8] we have shown that the matrix-associated cells are mainly macrophages, endothelial cells, and stromal cells in both uveal and xenografted melanoma. In addition, it appeared that murine cells were hardly present inside the tumor cells nests in melanoma xenografts, indicating that that infiltration of host cells is limited to the ECM patterns. These data indicate that these patterns may facilitate entrance of host cells into the tumor and perhaps also allow tumor cells to escape from the tumor, explaining thereby the higher degree of malignancy. Furthermore, the presence of nontumor cells along the matrix patterns raises the question of whether ECM patterns are assembled by stromal cells, melanoma cells, or both. ECM patterns can be generated by tumor cells in absence of fibroblasts or endothelial cells in vitro.[6,15,34,35] These data strongly suggest that the ECM patterns are primarily generated by tumor cells. In vivo, ECM-associated cells such as fibroblasts may subsequently deposit ECM compounds. In addition, expression of angiogenic proteins by tumor cells may induce the outgrowth of blood vessels in the ECM patterns. In any case, they seem to be induced primarily by the presence of the tumor cells and are therefore fundamentally different from a preexistent stroma that a tumor lesion invades. It may be hypothesized that melanoma cells deposit ECM around small nests of tumor cells; that they subsequently become infiltrated by different types of cells, including endothelial cells, fibroblasts, and macrophages; and, finally, that these latter cells contribute to further remodeling, maturation, and expansion of the patterns.[6,15] In this respect, it is remarkable that collagen III is absent (besides the microvasculature), because collagen III is a regular component of reticulin.

Recently, it has been posited that involvement of fibroblasts in melanoma growth and progression probably occurs through several stages, including conversion to myofibroblasts.[42] In this respect, it is interesting that muscle actin staining was negative in the uveal melanoma lesions, suggesting the absence of myofibroblasts. Indeed, the role of myofibroblasts in the formation and maturation of the ECM patterns may be limited. Otherwise, it is possible that they had already differentiated into mature fibroblasts.

Recently, similar ECM patterns were visualized in vivo by indocyanine green angiography in patients with uveal melanoma and a rabbit model.[6,43,44] An angiographic–histologic correlation confirmed the identity of the angiographic patterns. Because we demonstrated close parallels between the xenograft model and uveal melanoma, it is likely that our results are representative of the observations obtained in clinical studies.

Exudative retinal detachment is present in most uveal melanomas, and it is the most common complication of these tumors. Recently, the presence of ECM patterns (besides tumor

**TABLE 2.** Immunohistochemical Analysis of the Separate Uveal Melanoma Lesions

| | Arcs, Loops, and Network Patterns | | | Microvasculature | | | Tumor Cells | | |
|---|---|---|---|---|---|---|---|---|---|
| **ECM Component** | **1** | **2** | **3** | **1** | **2** | **3** | **1** | **2** | **3** |
| Pan-HSPG | + | + | + | + | + | + | + | + | + |
| Heparan sulfate side chains | + | + | + | + | + | + | − | ± | − |
| Syndecan-2 | − | − | − | − | −/± | − | −/± | −/± | −/± |
| Syndecan-1 and -3 | − | − | −/± | − | −/± | − | + | + | + |
| Syndecan-3 | − | − | − | + | + | + | − | −/± | − |
| Glypican-1 | −/± | − | − | − | −/± | − | ± | ± | ± |
| Agrin | + | + | + | + | + | + | − | − | − |
| Perlecan | + | + | + | + | + | + | − | − | − |
| Collagen XVIII | + | + | + | + | + | + | − | − | − |
| Collagen I | + | + | + | + | + | + | − | − | − |
| Collagen III | − | − | − | ± | ± | ± | − | − | − |
| Collagen IV | + | + | + | + | + | + | − | − | − |
| Collagen V | + | + | + | + | + | + | − | − | − |
| Reticulin | + | + | + | + | + | + | − | − | − |

Intensity of staining was scored as negative (−, Fig. 3A), weak (±, Fig. 3I) or strong (+, Fig. 3B). 1, 2, and 3 indicate the separate lesions.

size) was said to be related to the presence of exudative retinal detachment.[45] No satisfactory explanation was provided to explain the occurrence of this detachment. As depicted in Figure 4, leakage of exudate-like fluid from the patterns could offer an explanation for this phenomenon.

In conclusion, our data suggest that the ECM arcs, loops, and network patterns accommodate the transport of plasma-derived molecules (oxygen and nutrients) into the tumor lesion, thereby enhancing tumor growth and progression and facilitating infiltration of tumor tissue by host-derived cells. The amount of delivery of oxygen in avascular regions in the tumor may be very limited, since only low amounts of oxygen are carried by plasma. Therefore, the exudate present in the ECM arcs, loops, and network patterns probably predominantly carries small-sized molecules such as glucose and other nutrients.

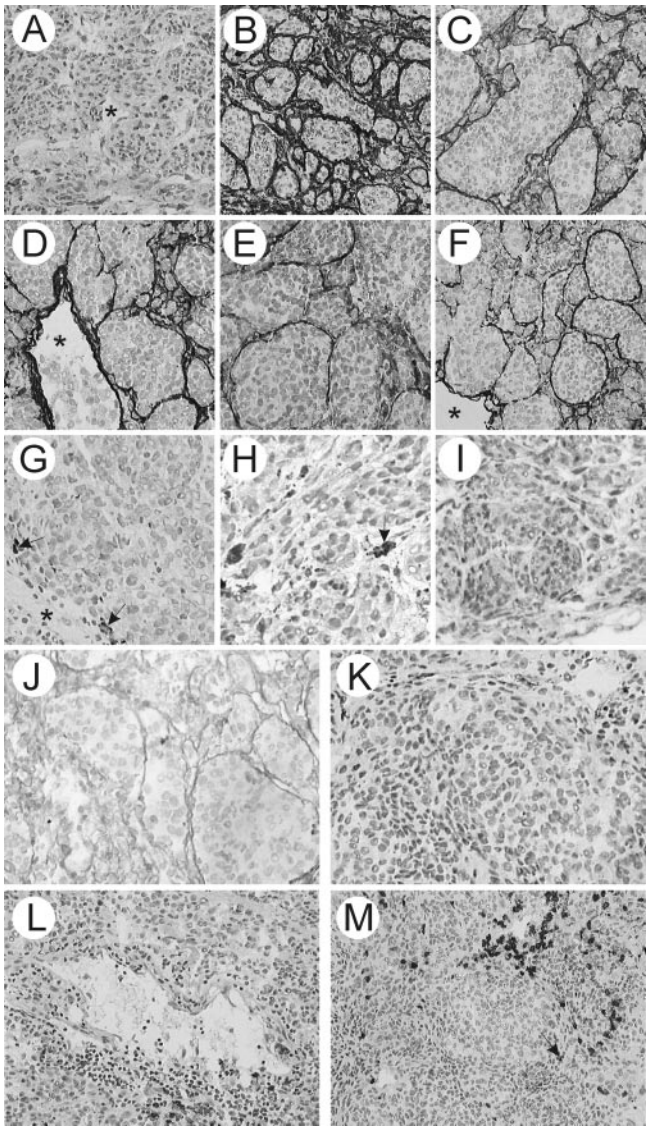


**FIGURE 3.** Immunohistochemical analysis of the expression of collagen III (**A**), collagen IV (**B**), collagen V (**C**), collagen XVIII (**D**), agrin (**E**), perlecan (**F**), syndecan-1 and -3 (**G**), syndecan-2 (**H**), glypican-1 (**I**), and reticulin (**J**) and the presence of pericytes (anti-α-SM1 mAb, **K**), B-lymphocytes (anti-CD20 mAb; **L**), and T-lymphocytes (anti-CD3 mAb; **M**) in primary uveal melanoma. (**A**, **D**, **F**, **G**; ✶) Blood vessel lumina; (**G**, **H**; *arrows*) and syndecan-positive stromal cells (possibly macrophages). (**L**) B-cells adjacent to a large blood vessel. (**M**) T-cells were occasionally associated with the ECM arcs, loops, and network patterns (*arrow*). Counterstain, Harris' hematoxylin. Magnification: (**A**–**F**, **I**, **J**, **L**, **M**) ×200; (**G**, **H**, **K**) ×400.

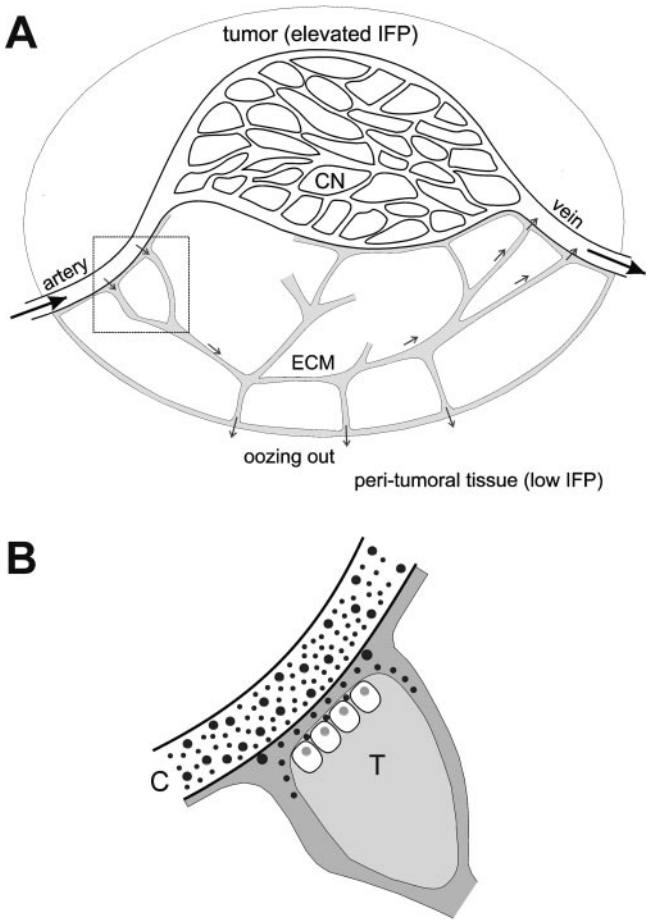


**FIGURE 4.** A hypothetical mechanism of perfusion in tumors containing the arcs, loops, and network patterns. (**A**) Blood flow is conducted by the artery, via the capillary network (CN) toward the venous vessel (*large arrows*). Exudate-like fluid moves across an arterial microvessel wall (*small arrows*) into the ECM in tumor areas where arterial pressure exceeds interstitial fluid pressure. ECM patterns conduct the exudate-like fluid toward the venous microvasculature (*small arrows*) where blood pressure is lower than the elevated interstitial fluid pressure,[37] causing re-entry into the blood stream. Also, leakage into peritumoral tissue (in which the interstitial fluid pressure is approximately 0 mm Hg[38]) or the subretinal space (and subsequently via the retina into the vitreous body) in cases of uveal melanoma (i.e., oozing out) may occur. Although the schematic suggests that the two systems—blood vasculature and ECM patterns—are physically separated, their interconnections are numerous and scattered all over the tumor tissue. The *boxed area* in (**A**) is magnified in (**B**), showing leakage of the exudate-like fluid containing small and large sized molecules (represented by *small* and *large dots*) from the blood vasculature into the ECM compartment. Deep infiltration of large molecules is limited. Only small molecules are able to penetrate the ECM patterns fully and also in small amounts between the tumor cells lining these patterns (T, tumor; C, capillary).

## *Acknowledgments*

The authors thank Geert Poelen and Debby Smits (Central Animal Laboratory, Nijmegen) for excellent assistance during the animal experiments and Jack van Horssen (Department of Pathology) and Ritva Pihlajaniemi (Department of Medical Biochemistry and Molecular Biology, University of Oulu, Finland) for providing antibodies for HSPG detection.

## *References*


1. Folberg R, Pe'er J, Gruman LM, et al. The morphologic characteristics of tumor blood vessels as a marker of tumor progression in primary human uveal melanoma. *Hum Pathol*. 1992;23:1298–1305.
2. Folberg R, Rummelt V, Parys van Ginderdeuren R, et al. The prognostic value of tumor blood vessel morphology in primary uveal melanoma. *Ophthalmology.* 1993;100:1389–1398.
3. Warso MA, Maniotis AJ, Chen X, et al. Prognostic significance of periodic acid-Schiff-positive patterns in primary cutaneous melanoma. *Clin Cancer Res*. 2001;7:473–477.
4. Thies A, Mangold U, Moll I, Schumacher U. PAS-positive loops and networks as a prognostic indicator in cutaneous malignant melanoma. *J Pathol*. 2001;195:537–542.
5. Mäkitie T, Summanen P, Tarkkanen A, Kivelä T. Microvascular loops and networks as prognostic indicators in choroidal and ciliary body melanomas. *J Natl Cancer Inst*. 2000;91:359–367.
6. Maniotis AJ, Folberg R, Hess A, et al. Vascular channel formation by human melanoma cells in vivo and in vitro: vasculogenic mimicry. *Am J Pathol.* 1999;155:739–752.
7. Hendrix MJ, Seftor EA, Hess AR, Seftor RE. Vasculogenic mimicry and tumour-cell plasticity: lessons from melanoma. *Nat Rev Cancer*. 2003;3:411–421.
8. Clarijs R, Otte-Höller I, Ruiter DJ, de Waal RM. Presence of a fluid-conducting meshwork in xenografted cutaneous and primary human uveal melanoma. *Invest Ophthalmol Vis Sci*. 2002;43:912–918.
9. Daniels KJ, Boldt HC, Martin JA, Gardner LM, Meyer M, Folberg R. Expression of type VI collagen in uveal melanoma: its role in pattern formation and tumor progression. *Lab Invest*. 1996;75:55–66.
10. Mäkitie T, Summanen P, Tarkkanen A, Kivelä T. Tumor-infiltrating macrophages (cd68(+) cells) and prognosis in malignant uveal melanoma. *Invest Ophthalmol Vis Sci*. 2001;42:1414–1421.
11. Mäkitie T, Tarkkanen A, Kivelä T. Comparative immunohistochemical oestrogen receptor analysis in primary and metastatic uveal melanoma. *Graefes Arch Clin Exp Ophthalmol*. 1998;236:415–419.
12. Leek RD, Lewis CE, Whitehouse R, Greenall M, Clarke J, Harris AL. Association of macrophage infiltration with angiogenesis and prognosis in invasive breast carcinoma. *Cancer Res*. 1996;56:4625–4629.
13. Takanami I, Takeuchi K, Kodaira S. Tumor-associated macrophage infiltration in pulmonary adenocarcinoma: association with angiogenesis and poor prognosis. *Oncology*. 1999;57:138–142.
14. Vacca A, Ribatti D, Ruco L, et al. Angiogenesis extent and macrophage density increase simultaneously with pathological progression in B-cell non-Hodgkin's lymphomas. *Br J Cancer*. 1999;79:965–970.
15. Maniotis AJ, Chen X, Garcia C, et al. Control of melanoma morphogenesis, endothelial survival, and perfusion by extracellular matrix. *Lab Invest.* 2002;82:1031–1043.
16. Folberg R, Hendrix MJ, Maniotis AJ. Vasculogenic mimicry and tumor angiogenesis. *Am J Pathol*. 2000;156:361–381.
17. Clarijs R, Schalkwijk L, Ruiter DJ, de Waal RM. Lack of lymphangiogenesis despite coexpression of VEGF-C and its receptor Flt-4 in primary uveal melanoma. *Invest Ophthalmol Vis Sci*. 2001;42:1422–1428.
18. Westphal JR, van't Hullenaar RG, van der Laak JA, et al. Vascular density in melanoma xenografts correlates with vascular permeability factor expression but not with metastatic potential. *Br J Cancer*. 1997;76:561–570.
19. van Muijen GN, Cornelissen LM, Jansen CF, et al. Antigen expression of metastasizing and non-metastasizing human melanoma cells xenografted into nude mice. *Clin Exp Metastasis*. 1991;9:259–272.
20. Pötgens AJ, van Altena MC, Lubsen NH, Ruiter DJ, de Waal RM. Analysis of the tumor vasculature and metastatic behavior of xenografts of human melanoma cell lines transfected with vascular permeability factor. *Am J Pathol*. 1996;148:1203–1217.
21. David G, Bai XM, Van der Schueren B, Cassiman JJ, Van den Berghe H. Developmental changes in heparan sulfate expression: in situ detection with mAbs. *J Cell Biol*. 1992;119:961–975.
22. van den Born J, Gunnarsson K, Bakker MA, et al. Presence of N-unsubstituted glucosamine units in native heparan sulfate revealed by a monoclonal antibody. *J Biol Chem*. 1995;270:31303–31309.
23. David G, Bai XM, Van der Schueren B, Marynen P, Cassiman JJ, Van den Berghe H. Spatial and temporal changes in the expression of fibroglycan (syndecan-2) during mouse embryonic development. *Development*. 1993;119:841–854.
24. Lories V, Cassiman JJ, Van den Berghe H, David G. Multiple distinct membrane heparan sulfate proteoglycans in human lung fibroblasts. *J Biol Chem*. 1989;264:7009–7016.
25. Lories V, Cassiman JJ, Van den Berghe H, David G. Differential expression of cell surface heparan sulfate proteoglycans in human mammary epithelial cells and lung fibroblasts. *J Biol Chem*. 1992;267:1116–1122.
26. David G, Lories V, Decock B, Marynen P, Cassiman JJ, Van den Berghe H. Molecular cloning of a phosphatidylinositol-anchored membrane heparan sulfate proteoglycan from human lung fibroblasts. *J Cell Biol*. 1990;111:3165–3176.
27. de Boeck H, Lories V, David G, Cassiman JJ, Van den Berghe H. Identification of a 64 kDa heparan sulphate proteoglycan core protein from human lung fibroblast plasma membranes with a monoclonal antibody. *Biochem J*. 1987;247:765–771.
28. van den Born J, van den Heuvel LP, Bakker MA, Veerkamp JH, Assmann KJ, Berden JH. Monoclonal antibodies against the protein core and glycosaminoglycan side chain of glomerular basement membrane heparan sulfate proteoglycan: characterization and immunohistological application in human tissues. *J Histochem Cytochem*. 1994;42:89–102.
29. Saarela J, Rehn M, Oikarinen A, Autio-Harmainen H, Pihlajaniemi T. The short and long forms of type XVIII collagen show clear tissue specificities in their expression and location in basement membrane zones in humans. *Am J Pathol*. 1998;153:611–626.
30. Saarela J, Ylikarppa R, Rehn M, Purmonen S, Pihlajaniemi T. Complete primary structure of two variant forms of human type XVIII collagen and tissue-specific differences in the expression of the corresponding transcripts. *Matrix Biol*. 1998;16:319–328.
31. Tsukada T, Tippens D, Gordon D, Ross R, Gown AM. HHF35, a muscle-actin-specific monoclonal antibody. I. Immunohistochemical and biochemical characterization. *Am J Pathol*. 1987;126:51–60.
32. Tsukada T, McNutt MA, Ross R, Gown AM. HHF35, a muscle actin-specific monoclonal antibody. II. Reactivity in normal, reactive and neoplastic human tissues. *Am J Pathol*. 1987;127:389–402.
33. Clasper S, Vekemans S, Fiore M, et al. Inducible expression of the cell surface heparan sulfate proteoglycan syndecan-2 (fibroglycan) on human activated macrophages can regulate fibroblast growth factor action. *J Biol Chem*. 1999;274:24113–24123.
34. Sharma N, Seftor RE, Seftor EA, et al. Prostatic tumor cell plasticity involves cooperative interactions of distinct phenotypic subpopulations: role in vasculogenic mimicry. *Prostate*. 2002;50:189–201.
35. Sood AK, Seftor EA, Fletcher MS, et al. Molecular determinants of ovarian cancer plasticity. *Am J Pathol*. 2001;158:1279–1288.
36. Sunderkotter C, Steinbrink K, Goebeler M, Bhardwaj R, Sorg C. Macrophages and angiogenesis. *J Leukoc Biol*. 1994;55:410–422.
37. Boucher Y, Baxter LT, Jain RK. Interstitial pressure gradients in tissue-isolated and subcutaneous tumors: implications for therapy. *Cancer Res*. 1990;50:4478–4484.
38. Roh HD, Boucher Y, Kalnicki S, Buchsbaum R, Bloomer WD, Jain RK. Interstitial hypertension in carcinoma of uterine cervix in patients: possible correlation with tumor oxygenation and radiation response. *Cancer Res*. 1991;51:6695–6698.
39. Granath KA, Kvist BE. Molecular weight distribution analysis by gel chromatography on Sephadex. *J Chromatogr*. 1967;28:69–81.
40. Jain RK. Transport of molecules in the tumor interstitium: a review. *Cancer Res*. 1987;47:3039–3051.

41. Lin K, Nagy JA, Xu H, Shockley TR, Yarmush ML, Dvorak HF. Compartmental distribution of tumor-specific monoclonal antibodies in human melanoma xenografts. *Cancer Res*. 1994;54:2269–2277.
42. Ruiter D, Bogenrieder T, Elder D, Herlyn M. Melanoma-stroma interactions: structural and functional aspects. *Lancet Oncol*. 2002;3:35–43.
43. Mueller AJ, Bartsch DU, Folberg R, et al. Imaging the microvasculature of choroidal melanomas with confocal indocyanine green scanning laser ophthalmoscopy. *Arch Ophthalmol.* 1998; 31–39.
44. Mueller AJ, Folberg R, Freeman WR, et al. Evaluation of the human choroidal melanoma rabbit model for studying microcirculation patterns with confocal ICG and histology. *Exp Eye Res*. 1999;68: 671–678.
45. Kivelä A, Eskelin S, Mäkitie T, Summanen P. Exudative retinal detachment from malignant uveal melanoma: predictors and prognostic significance. *Invest Ophthalmol Vis Sci*. 2001;42:2085–2093.